

# Preconfigured, Skewed Distribution of Firing Rates in the Hippocampus and Entorhinal Cortex

Kenji Mizuseki<sup>1,2,\*</sup> and György Buzsáki<sup>1,\*</sup>

<sup>1</sup>NYU Neuroscience Institute, Langone Medical Center, New York University, New York, NY 10016, USA

<sup>2</sup>Allen Institute for Brain Science, Seattle, WA 98103, USA

\*Correspondence: kenji.mizuseki@gmail.com (K.M.), gyorgy.buzsaki@nyumc.org (G.B.)

<http://dx.doi.org/10.1016/j.celrep.2013.07.039>

This is an open-access article distributed under the terms of the Creative Commons Attribution License, which permits unrestricted use, distribution, and reproduction in any medium, provided the original author and source are credited.

## SUMMARY

Despite the importance of the discharge frequency in neuronal communication, little is known about the firing-rate patterns of cortical populations. Using large-scale recordings from multiple layers of the entorhinal-hippocampal loop, we found that the firing rates of principal neurons showed a lognormal-like distribution in all brain states. Mean and peak rates within place fields of hippocampal neurons were also strongly skewed. Importantly, firing rates of the same neurons showed reliable correlations in different brain states and testing situations, as well as across familiar and novel environments. The fraction of neurons that participated in population oscillations displayed a lognormal pattern. Such skewed firing rates of individual neurons may be due to a skewed distribution of synaptic weights, which is supported by our observation of a lognormal distribution of the efficacy of spike transfer from principal neurons to interneurons. The persistent skewed distribution of firing rates implies that a preconfigured, highly active minority dominates information transmission in cortical networks.

## INTRODUCTION

The dominant communication across neurons occurs via spikes. Yet, despite the central role of spiking activity in transmitting information, only limited data about the firing rates of unbiased neuronal populations in intact networks are available (Hromádka et al., 2008; O’Connor et al., 2010). It is generally assumed that cortical principal cells fire sparsely, involving only a small percentage of spiking neurons in most situations while the majority of the population remains silent (Levy and Baxter, 1996; Wolfe et al., 2010). The term “sparse coding” refers to a model in which a small fraction of neurons is engaged in any situation, as opposed to a dense population code in which the firing-rate fluctuations of individual members represent the input (Olshausen and Field, 1997). In this postulated high signal-to-noise ratio scheme, slow-firing neurons contribute largely unwanted noise, which is viewed as an inevitable consequence of brain organiza-

tion (Lisman, 1997; Shadlen and Newsome, 1998) rather than information. In one possible solution for sparse coding, a small fraction of cortical neurons are active under diverse circumstances, but the active subset varies flexibly across brain states and situations. Alternatively, a largely heterogeneous group of neurons in each cortical layer may form a “skeleton” network in which firing rates are largely determined by the intrinsic properties of individual neurons and/or their distinct wiring. Under the latter scenario, largely the same fraction of cells would be active under all conditions and the information carried by their spikes could be represented by the deviation of their firing rate or timing from an overall default pattern. To determine whether cortical networks deploy an egalitarian or an inequitable solution, we must first have quantitative knowledge about the firing-rate distributions of unbiased populations in different conditions (Barth and Poulet, 2012).

Firing patterns in the hippocampus and entorhinal cortex (EC) are affected by a variety of factors. Place cells of the hippocampus fire clusters of spikes in their typically singular place fields (O’Keefe and Nadel, 1978), whereas grid cells in the EC have multiple fields that form a periodic triangular array, or grid (Hafting et al., 2005). However, little is known about the mechanisms that control the firing-rate distribution in the population. A main reason for this caveat is that definitions of the various spatial and nonspatial features are typically based on an experimenter-determined threshold and, as a consequence, neurons with low rates are often excluded because, viewed one by one, they typically do not yield statistically reliable behavioral correlations (Krupic et al., 2012). Thus, it has remained unclear whether the “representative” examples reflect the mean behavior of a homogeneous neuronal population or the high end of a heterogeneous distribution. It is essential to address this question in order to understand the nature of communication across neuron populations (Battaglia et al., 2005; Hromádka et al., 2008; Barth and Poulet, 2012; Song et al., 2005; Ikegaya et al., 2012; Yassin et al., 2010). Using a large database of physiologically characterized neurons (Mizuseki et al., 2009, 2011, 2012; Pastalkova et al., 2008; Diba and Buzsáki, 2008), we examined the firing-rate distributions of principal cells and putative interneurons in the main layers of the EC and hippocampal subregions in waking and sleeping rats. The analyses revealed a strongly skewed distribution of neuronal firing rates in all subregions that remained largely similar across different brain states and testing environments.

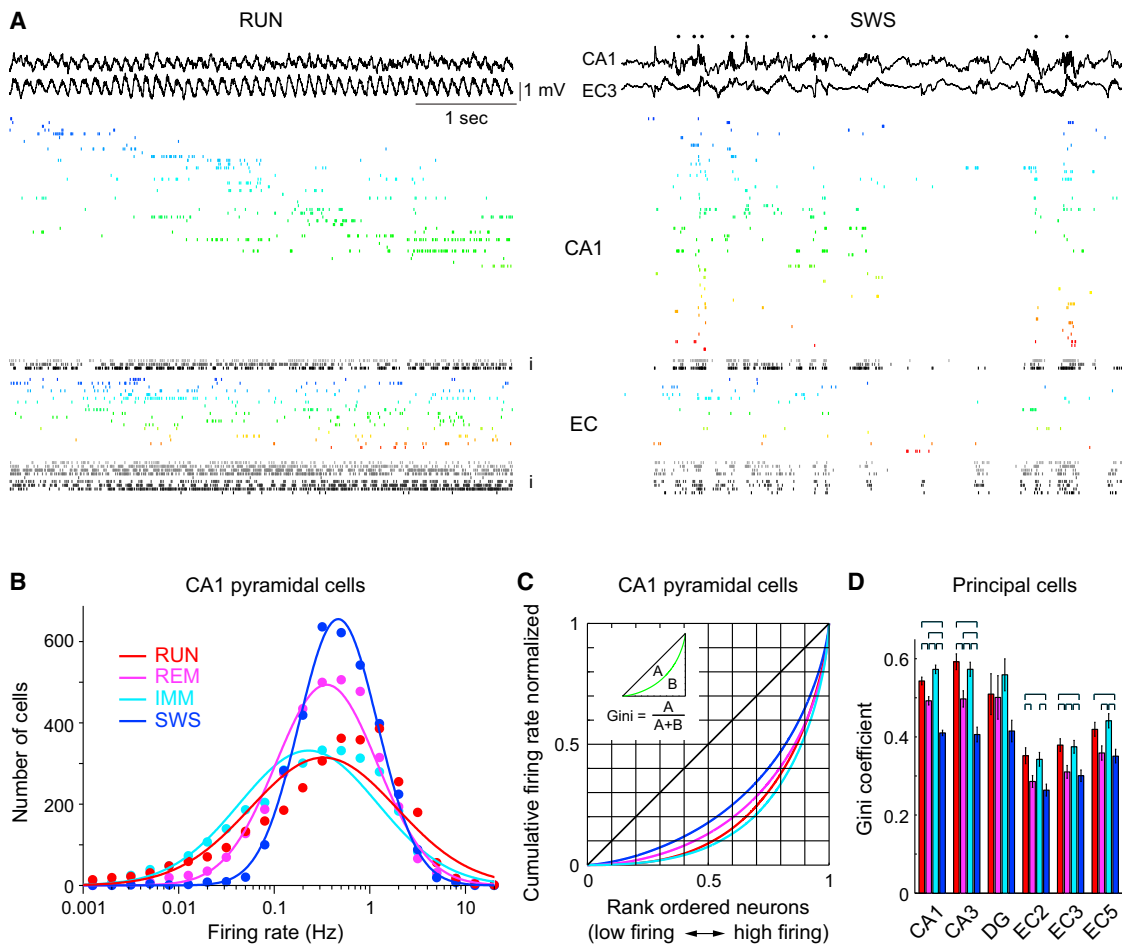


**Figure 1. Lognormal Firing-Rate Distribution of Principal Cells**

(A) LFP and spiking activity of CA1 and EC neurons. Dots above the CA1 LFP during SWS represent ripple oscillations. Note trains of spikes followed by long silence periods in the waking rat and strong population synchrony during ripples. Colored ticks: principal neurons; gray and black ticks (i): interneurons.

(B) Distribution of firing rates of individual CA1 pyramidal cells in different brain states. Note log x axis. Distribution during RUN extends to both left and right relative to SWS. Dots: data; lines: lognormal fit.

(C) Lorenz plots of the distribution of firing rates. Inset: Illustration of the Gini coefficient, which is determined by dividing A (the area between the line of equity and the Lorenz curve) by the areas marked with A and B.

(D) Gini coefficients in different hippocampal regions and EC layers in different brain states (mean  $\pm$  SEM). Brackets indicate significant differences ( $p < 0.05$ ; ANOVA, followed by Tukey's test).

(B–D) The same color codes for brain states are used.

See also Figure S1.

## RESULTS

Analyses were performed on a database of 7,327 neurons in the EC and hippocampus of 11 rats. Local field potentials (LFPs) and unit firing were recorded by multiple-shank silicon probes (Mizuseki et al., 2009; Fujisawa et al., 2008) from the hippocampal CA1 and CA3 pyramidal layers and dentate gyrus (DG). In four animals, recordings were made simultaneously in CA1 and in multiple layers of the medial EC. Histological localization of the electrodes, criteria for clustering of single units, and separation of principal neurons and interneurons in these animals were previously described in detail (Mizuseki et al., 2009; Diba and Buzsáki, 2008). Recordings were carried out while the animal ran on various maze configurations (Mizuseki et al., 2009,

2011, 2012; Pastalkova et al., 2008; Diba and Buzsáki, 2008) and theta periods from all maze behaviors were lumped together as “RUN.” Periods without theta were concatenated as immobility or consummatory behaviors (IMMs). Additional recordings were carried out during sleep, including several epochs of rapid eye movement (REM) sleep and slow wave sleep (SWS) in the animal’s home cage (Mizuseki et al., 2011, 2012).

### Long-Tail, Skewed Distribution of Firing Rates of Principal Cells and Interneurons

Both hippocampal and EC neurons showed characteristic population firing patterns during different brain states (Figure 1A; Csicsvari et al., 1999), but the directions of rate changes differed

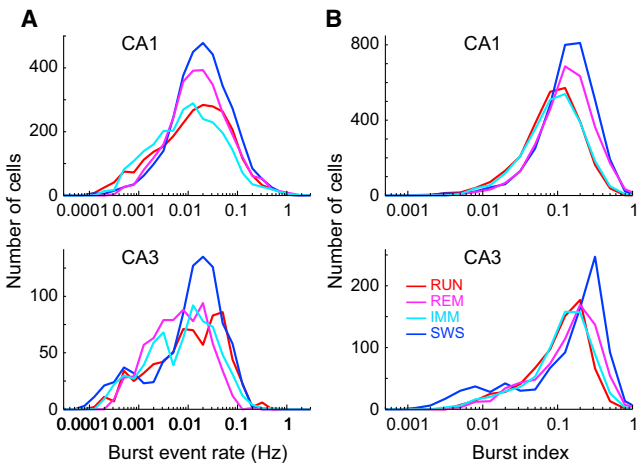


**Figure 2. Spike Bursts of Principal Cells in Different Brain States**

(A) Distribution of burst-event rates of individual CA1 and CA3 pyramidal cells in different brain states (three spikes or more at  $\leq 8$  ms intervals).  
(B) Distribution of burst indexes (number of spikes in bursts divided by the number of all spikes) of individual CA1 and CA3 pyramidal cells in different brain states.

See also Figure S2.

between the two regions. Whereas the overall rates of hippocampal principal neurons were lowest during REM sleep, EC neurons fired maximally during REM (Figure S1). A comparison of individual principal neurons revealed a three orders of magnitude range of the mean firing rates from 0.001 Hz to 10 Hz (Figure 1). The firing-rate distribution of CA1 pyramidal cells strongly deviated from Gaussian and showed an excellent fit to lognormal pattern during SWS. The distributions of log firing rate during other brain states were asymmetric, with long and heavy tails toward lower frequencies (Figure 1B). The right tail also extended significantly toward higher rates during RUN (the proportion of  $>2$  Hz neurons is largest during RUN; RUN = 12.3%, REM = 6.0%, IMM = 7.1%, SWS = 5.7%; chi-square test,  $p < 0.00001$ ).

Firing-rate inequality among individual neurons can be quantitatively described by Lorenz statistics (O'Connor et al., 2010; Ikegaya et al., 2012). The Lorenz curve of the firing-rate distribution characterizes the cumulative spike share of individual neurons of the population, as shown in Figure 1C. In this display, the diagonal ( $x = y$ ) indicates that all neurons have the same firing rate. The magnitude of the deviation from equality is quantified by the Gini coefficient (Figure 1C, inset); the higher the coefficient, the more unequal is the share of the number of spikes (Ikegaya et al., 2012). For example, during RUN, 70.4% of the recorded CA1 pyramidal cells had a mean rate of  $<1$  Hz, whereas a small fraction of strongly active pyramidal cells (13.3%) contributed to 50% of all spikes. Remarkably, the brain-state dependence of the firing-rate inequality was similar for the principal cells in all regions of the hippocampus and all layers of the EC, i.e., Gini coefficients were higher during awake states (RUN and IMM) than during sleep states (REM and SWS; Figure 1D). The firing-rate distributions in all regions and layers across behaviors are shown in Figure S1. In summary, the firing rates of

hippocampal and EC principal neurons displayed strongly skewed firing-rate distributions, with the widest frequency range of individual neurons in waking animals.

### Skewed Distribution of Spike Bursts of Principal Cells

In addition to single spikes, pyramidal neurons also fire complex spike bursts. It has been suggested that generation of bursts is enhanced under special conditions (Harris et al., 2001), and that bursts play a distinct role in plasticity (Magee and Johnston, 1997; Thomas et al., 1998; Pike et al., 1999, Harris et al., 2001) and computation (Lisman, 1997; Thomson, 2000). Therefore, revealing the burst-event rate of unbiased neuronal populations is essential for understanding their role in circuit operations. Burst is defined here as a series of three or more spikes with  $<8$  ms interspike intervals (Harris et al., 2001; Mizuseki et al., 2012). The burst-event rate of individual neurons also showed a lognormal-like distribution (Figure 2A), as did the distribution of the burst index, defined as the ratio of spikes within bursts to all spikes (Mizuseki et al., 2012; Figure 2B). The burst index was highest during SWS for all EC and hippocampal principal cells (Figure S2A;  $p < 0.05$  for all brain regions but the DG; Kruskal-Wallis ANOVA, followed by Tukey's honestly significant difference test). A small fraction of CA1 (RUN = 0.4%, REM = 3.1%, IMM = 0.5%, SWS = 2.9%) and CA3 (RUN = 0.8%, REM = 2.1%, IMM = 0.9%, SWS = 4.1%) pyramidal cells were "superbursters," since  $>50\%$  of the spikes they emitted were classified as bursts. The burst index was weakly but significantly correlated with the firing rate ( $p < 0.011$ ; Figures S2B and S2C). Essentially identical results were obtained using  $<6$  ms or  $<10$  ms interspike intervals for the identification of burst events.

### Skewed Distribution of Hippocampal Place Cell Firing

The spontaneous and evoked firing patterns of cortical neurons are often dramatically different, although these patterns may be related to each other. Since place-related firing can be conceived of as a specific, environment-driven activity (O'Keefe and Nadel, 1978), we examined the place-related activity of pyramidal cells at increasing levels of criteria. Place fields on the open field were first defined as a continuous region of at least  $225 \text{ cm}^2$  (nine bins) in which the firing rate was above 10% (or 20%) of the peak firing rate. Restricted subsets of these groups included only place fields with spatial coherence (Muller and Kubie, 1989) greater than 0.7 (Hafting et al., 2008; Mizuseki et al., 2009). The spatial coherence of each firing field was defined as the correlation of the firing rate in each bin of the firing field with the firing rate in its neighboring bins to measure local smoothness of firing rate in space (Muller and Kubie, 1989). These two steps of restriction created four subgroups of place cells with the highest (20% and 0.7 spatial coherence) to lowest (10% and no spatial coherence restriction) quality of place fields. Irrespective of how we defined the place fields, the mean within-field firing rates of CA1 and CA3 pyramidal cells showed a skewed distribution (Figures 3A and S3). Only 4.6% of CA1 pyramidal cells (8.4% CA3) sustained  $\geq 10$  Hz within-field rates, whereas the majority (89.6% CA1; 71.4% CA3) fired below the mean theta frequency ( $\sim 8$  Hz). Within-place field peak firing rates also displayed a skewed rate distribution (Figures 3B and S3). Within-field and peak rates were strongly correlated (CA1,

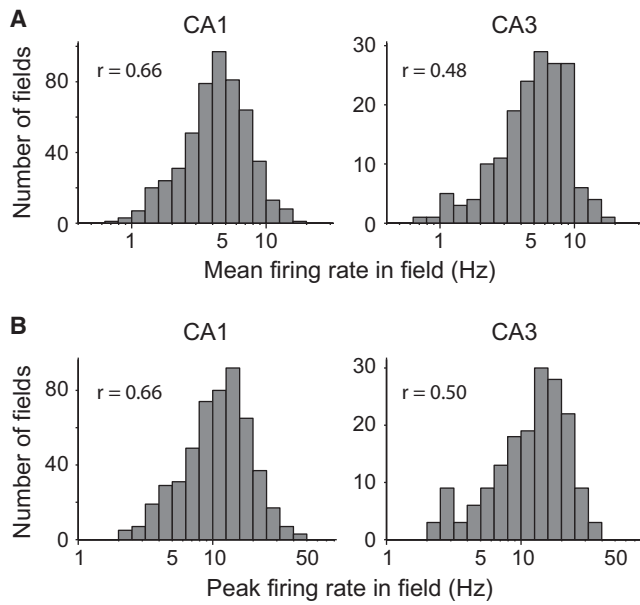


**Figure 3. Distribution of Firing Rates in Place Cells**

(A) Distribution of mean within-field firing rates of CA1 and CA3 pyramidal cells on the square maze.  
 (B) Distribution of peak firing rates in field.  
 R values in panels, correlation coefficients between session (RUN) firing rate, and mean within-field rate or peak rate. Place fields were defined by >10% peak firing rate and >0.7 spatial coherence.  
 See also Figure S3.

$R = 0.85$ ; CA3,  $R = 0.78$ ;  $P < 0.00001$ ), as were the within-field versus session mean (CA1,  $R = 0.66$ ; CA3,  $R = 0.50$ ;  $P < 0.00001$ ) and peak rate versus session mean (CA1,  $R = 0.66$ ; CA3,  $R = 0.48$ ;  $P < 0.00001$ ) rates. Therefore, a skewed distribution of the firing rate is a fundamental feature of hippocampal neurons.

Since firing rates may be related to several features of place cells, we next examined the relationship between log rate and place features on the square maze. Cell firing stability, defined as the pixel-by-pixel correlation of firing rates in the first and second parts of a session, showed a significant and sigmoid-like relationship with the log firing rate (Figure 4A; CA1,  $R = 0.62$ ; CA3,  $R = 0.75$ ,  $P < 0.00001$ ). Similarly, the spatial coherence of firing also displayed a sigmoid-like relationship with the log firing rate (Figure 4B; CA1,  $R = 0.71$ ; CA3,  $R = 0.82$ ;  $P < 0.00001$ ). Another frequently used index, the information rate (bits per second) of spiking activity (Skaggs et al., 1993), a quantity that defines the relationship between spikes and the rat's position on the maze, was also strongly correlated with the log firing rate (Figure 4C; CA1,  $R = 0.73$ ; CA3,  $R = 0.76$ ;  $P < 0.00001$ ). Figure 4 shows both place cells (using the 10% and 0.7 spatial coherence definition; black circles) and other neurons (gray circles). As expected, very few neurons with low firing rates met the criteria of place cell definition. On the other hand, not all fast neurons were classified as place cells either. The correlation between the log rate of place cells and the information rate was also significant (CA1,  $R = 0.77$ ; CA3,  $R = 0.76$ ;  $P < 0.00001$ ). The correlation between the log rate of bona fide place cells and the

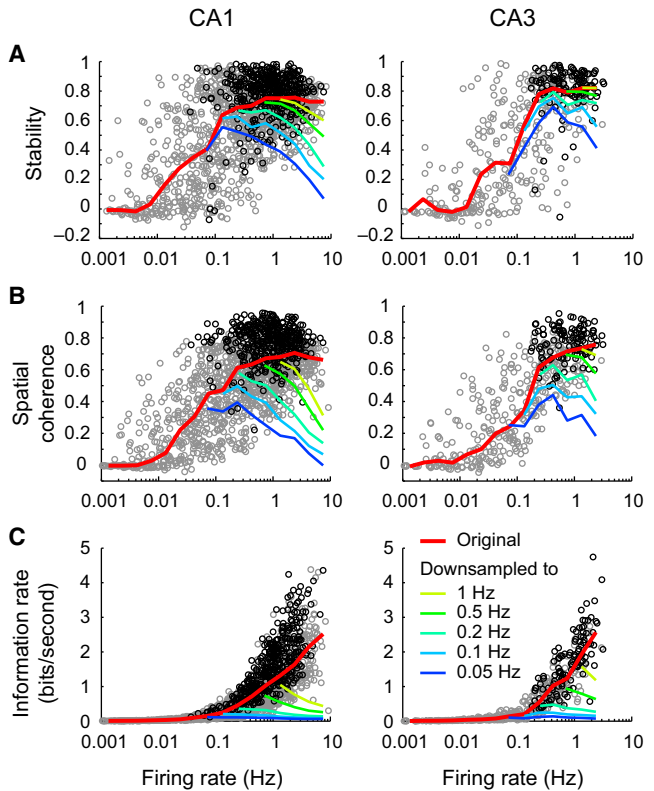


**Figure 4. Firing Rates Are Correlated with Spike Behavioral Measures**

(A) Relationship between log firing rate (RUN) and stability index (pixel-by-pixel correlation of rate between the first and second halves of a session in the square maze).  
 (B) Relationship between log firing rate (RUN) and spatial coherence.  
 (C) Relationship between log firing rate (RUN) and information rate.  
 Black circles: place cells (10%, 0.7 coherence criteria); gray circles: other neurons. Color lines indicate median values for original and downsampled rates. Only medians are shown for downsampled rates.  
 See also Figure S4.

stability of CA1 place cells was weaker but still significant ( $r = 0.16$ ,  $p < 0.001$ ).

Fast-firing neurons may acquire their advantage for spatial representation simply from their high rates. To test this possibility, we randomly thinned spikes for each fast-firing neuron so that the reduced rate was equal to 0.05 Hz to 1 Hz (Figure 4). Recomputing the analyses described above with the downsampled rates dramatically reduced the stability, spatial coherence, and information rate measures to or below the levels of the neurons that naturally fired at such frequencies (Figure 4). The magnitude of the loss from downsampling was proportional to the original frequency. Thus, fast-discharging neurons gain their efficacy from the high frequency of spikes they emit.

The firing rate was also correlated with the number of place fields (CA1,  $R = 0.22$ ; CA3,  $R = 0.39$ ;  $P < 0.00001$ ), place field size (CA1,  $R = 0.41$ ;  $p < 0.00001$ ; CA3,  $R = 0.25$ ;  $p < 0.001$ ), and phase precession (O'Keefe and Recce, 1993) slope (CA1,  $R = 0.11$ ;  $p < 0.05$ ; Figure S4), adding further support for the computational advantage of high rates of activity.

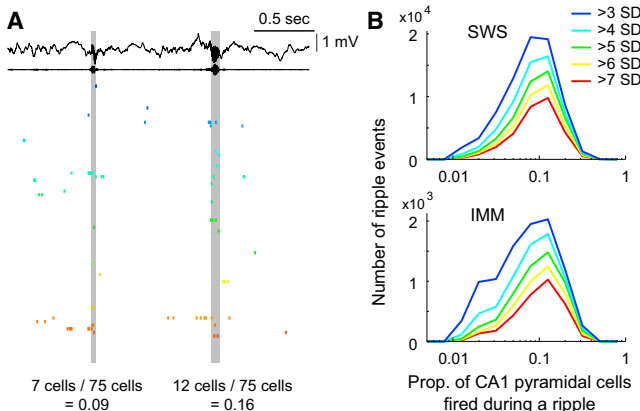


**Figure 5. Skewed Distribution of the Magnitude of Population Synchrony during Ripples**

(A) Wide-band and ripple band (140–230 Hz) filtered LFP (top) and spiking activity of simultaneously recorded 75 CA1 pyramidal cells. Two ripple events with relatively low (0.09) and high (0.16) fractions of neurons firing synchronously during ripples.

(B) Distribution of the synchrony of CA1 pyramidal cells' firing during ripples using various ripple detection thresholds (from small [ $>3$  SD] to large [ $>7$  SD]) during SWS and IMM.

See also Figure S5.

### Skewed Distribution of Population Synchrony

Another major network pattern in the EC-hippocampus is the self-organized sharp wave ripple (SPW-R, 140–180 Hz; [Buzsáki et al., 1992](#); [Csicsvari et al., 2000](#)). We used three indexes to examine the SPW-R-related firing patterns for each CA1 neuron during SWS or IMM: (1) the proportion of spikes during SPW-Rs, defined as the number of spikes during SPW-Rs divided by the number of all the spikes in that session; (2) the proportion of SPWs in which each neuron fired, calculated as the fraction of SPW-Rs in which the neuron fired at least once; and (3) the mean number of spikes per SPW-R. The number of spikes within SPW-Rs was divided by the total number of SPW-Rs in that session. Each of these indexes showed a lognormal-like distribution during both IMM and SWS ([Figure S5](#)). A small fraction (SWS = 1.4%, IMM = 1.5%) of CA1 pyramidal cells dominated by participating in 50% of SPW-R events, whereas half of all neurons fired in <10.6% (SWS; IMM < 9.1%) of SPW-Rs. The proportion of spikes during SPW-Rs was negatively correlated with the overall spike rate (SWS R = -0.12; IMM R = -0.56; Ps < 0.00001), indicating that slow-firing CA1 pyramidal cells emitted action potentials predominantly during SPW-R events, when the overall excitability of the EC-hippocampal networks is high ([Csicsvari et al., 2000](#)). The proportion of SPWs in which each neuron fired and the mean number of spikes per SPW-R were positively correlated with firing rates in both pyramidal cells and interneurons (R > 0.70; Ps < 0.00001). These results were essentially the same when the threshold for SPW-R selection was decreased from  $>7$  SD amplitude to  $>6$ ,  $>5$ ,  $>4$ , or  $>3$  SD above the mean.

Because SPW-Rs are self-organized events, they provided us the opportunity to examine how neurons with lognormal-like firing-rate statistics interact with each other at the population level. To that end, we computed the fraction of principal neurons

that fired at least one spike in each SPW-R ([Figure 5](#)), using five different groups of SPW-R magnitude (thresholds of  $>7$ ,  $>6$ ,  $>5$ ,  $>4$ , or  $>3$  SD above the mean). Only sessions with  $\geq 50$  simultaneously recorded CA1 pyramidal cells were included in these analyses (15 sessions with five animals). Independently of the applied threshold, the magnitude of SPW-R synchrony displayed a skewed distribution during both SWS and IMM ([Figure 5B](#)). Population synchrony of neurons was strongly correlated with the peak power (for  $>3$  SD events, SWS R = 0.45, IMM R = 0.49; Ps < 0.00001) or the mean power of the SPW-Rs (SWS R = 0.41, IMM R = 0.49; Ps < 0.00001).

To examine the distribution of population synchrony outside SPW-Rs, we plotted the proportion of principal neurons of CA1 and CA3 pyramidal cells that fired together in 10, 20, 50, 100, or 200 ms time bins. Similar to the analysis of synchrony during SPW-R events, the magnitude of population synchrony showed lognormal-like distribution in all brain states (data not shown). These findings demonstrate that the magnitude of neuronal synchrony during self-organized SPW-R and theta oscillations also follows lognormal statistics.

### Firing-Rate Correlations across Brain States and Testing Conditions

The small fraction of highly active neurons can vary from state to state, or the rate distribution may reflect a relatively “fixed” property of neurons ([Barth and Poulet, 2012](#)). To differentiate between these possibilities, we first compared the firing rates across different brain states. The firing rates of individual principal cells were robustly correlated between SWS and REM ([Figure 6A](#);  $R_{SWS-REM}$ , CA1 = 0.78, CA3 = 0.82, DG = 0.67, EC2 = 0.89, EC3 = 0.87, EC5 = 0.67; Ps < 0.00001, t test; [Csicsvari et al., 1999](#); [Hirase et al., 2001](#)) as well as across other states in all regions ( $R_{SWS-RUN}$ , CA1 = 0.57; CA3 = 0.65, DG = 0.74, EC2 = 0.23, EC3 = 0.28, EC5 = 0.33;  $R_{SWS-IMM}$ , CA1 = 0.58, CA3 = 0.66, DG = 0.82, EC2 = 0.23, EC3 = 0.33, EC5 = 0.37,  $R_{REM-RUN}$ , CA1 = 0.49, CA3 = 0.60, DG = 0.82, EC2 = 0.30, EC3 = 0.37, EC5 = 0.32;  $R_{REM-IMM}$ , CA1 = 0.50, CA3 = 0.57, DG = 0.82, EC2 = 0.26, EC3 = 0.39, EC5 = 0.31,  $R_{RUN-IMM}$ , CA1 = 0.90, CA3 = 0.89, DG = 0.88, EC2 = 0.94, EC3 = 0.94, EC5 = 0.89; Ps < 0.00001). In a second comparison, we tested the rate changes of CA1 and CA3 pyramidal cells while the animal successively performed in two different familiar mazes in the same room ([Figures 6B and S6](#); n = 6 rats; “rate remapping”; [Leutgeb et al., 2005](#)) or ran in opposite directions on a linear-track maze ([Figures 6D and S6](#); “global remapping”; [Leutgeb et al., 2005](#)). Again, we found that log firing rates of the neurons across the different testing situations were robustly conserved (CA1,  $R_{Maze\ A-Maze\ B} = 0.65$ ; CA3,  $R_{Maze\ A-Maze\ B} = 0.59$ , Ps < 0.00001) and between two directions of linear maze runs (CA1,  $R_{Left-Right} = 0.62$ ; CA3,  $R_{Left-Right} = 0.51$ , Ps < 0.00001). Even the correlation between linear firing rates was significant (CA1,  $R_{Maze\ A-Maze\ B} = 0.59$ , CA3,  $R_{Maze\ A-Maze\ B} = 0.26$ , Ps < 0.00001; CA1,  $R_{Left-Right} = 0.48$ , CA3,  $R_{Left-Right} = 0.20$ , Ps < 0.00001). In addition to firing rates, the burst index of neurons was also preserved across two different mazes ([Figure 6C](#); CA1,  $R_{Maze\ A-Maze\ B} = 0.63$ ; CA3,  $R_{Maze\ A-Maze\ B} = 0.57$ ; Ps < 0.00001). Finally, we compared log firing rates between familiar and novel environments. Log firing rates during RUN in familiar

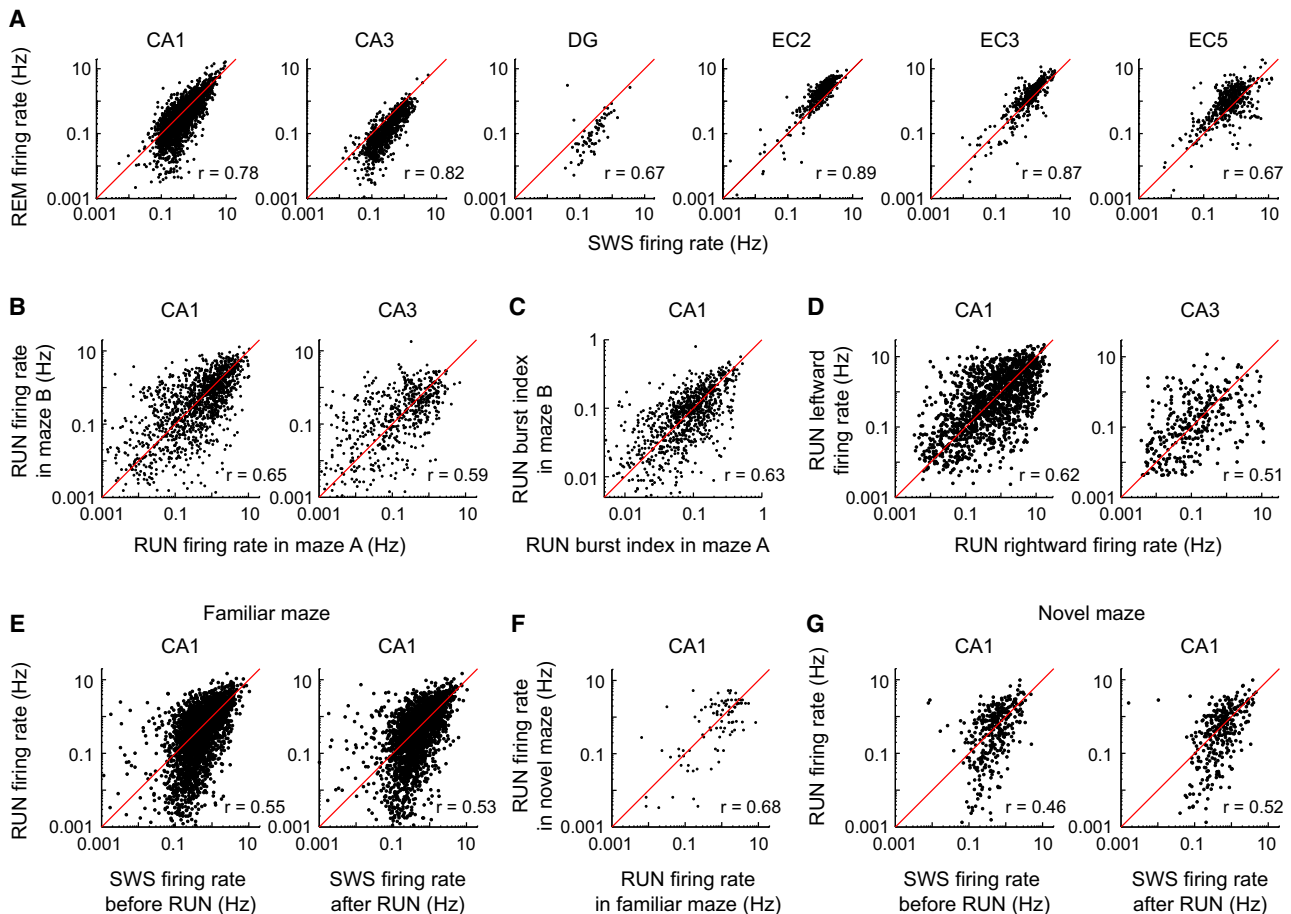


**Figure 6. Preserved Firing Rates of Principal Neurons across Brain States and Distinct Environments**

- (A) Comparison of firing rates of the same neurons during SWS and REM in different hippocampal regions and EC layers.
  - (B) Comparison of firing rates of the same neurons in different mazes.
  - (C) Comparison of burst indexes in different mazes.
  - (D) Comparison of firing rates during left and right runs on the linear track (“global remapping”).
  - (E) Firing-rate comparison between RUN in familiar maze and SWS in the home cage either before or after the maze session.
  - (F) Comparison of firing rates of the same neurons in familiar and novel mazes.
  - (G) Comparison between firing rates during exploration of a novel maze (RUN) and SWS in the home cage either before or after the maze session.
- (A–G) Each dot represents a single principal neuron. R values are correlation coefficients of log firing rates. All correlations were significant ( $p < 0.00001$ ). See also Figure S6.

and novel mazes were significantly correlated (Figure 6F; CA1,  $R_{\text{familiar-novel}} = 0.68$ ,  $p < 0.00001$ ; linear rate  $R_{\text{familiar-novel}} = 0.32$ ,  $p < 0.002$ , four sessions). A comparison between RUN and SWS both before and after the behavioral performance in the familiar maze (Figure 6E) also yielded significant log rate correlations (CA1,  $R_{\text{SWS before-RUN}} = 0.55$ ,  $R_{\text{SWS after-RUN}} = 0.53$ ; CA3,  $R_{\text{SWS before-RUN}} = 0.59$ ,  $R_{\text{SWS after-RUN}} = 0.61$ ;  $P < 0.00001$ ). Similarly, log firing rates were highly correlated between RUN and pre-RUN SWS or post-RUN SWS when exploration took place in a novel environment (Figure 6G; ten sessions with four animals, CA1  $R_{\text{SWS before-RUN}} = 0.46$ ,  $R_{\text{SWS after-RUN}} = 0.52$ ,  $P < 0.00001$ ; CA3  $R_{\text{SWS before-RUN}} = 0.59$ ,  $R_{\text{SWS after-RUN}} = 0.65$ ,  $P < 0.0005$ ). The largest variability across brain states occurred in the slow-firing population, since many of the slow-firing neurons during SWS became silent during RUN (Thompson and

Best, 1989). The significant rate correlations across states and testing environments, and especially between SWS before the novel experience and exploration of the novel environment, imply that the firing rate of individual neurons is relatively “fixed.”

#### Spike Transmission between Principal Neurons and Interneurons

Several computational models suggest that the lognormal distribution of synaptic strengths observed between neurons *in vitro* (Song et al., 2005) should give rise to skewed distributions of firing rates *in vivo* (Ikegaya et al., 2012; Koulakov et al., 2009; Roxin et al., 2011). Unfortunately, to date, no method exists for the direct measurement of synaptic strengths in a behaving animal. An indirect estimation can be obtained by quantifying the spike transmission probability between neuron pairs under

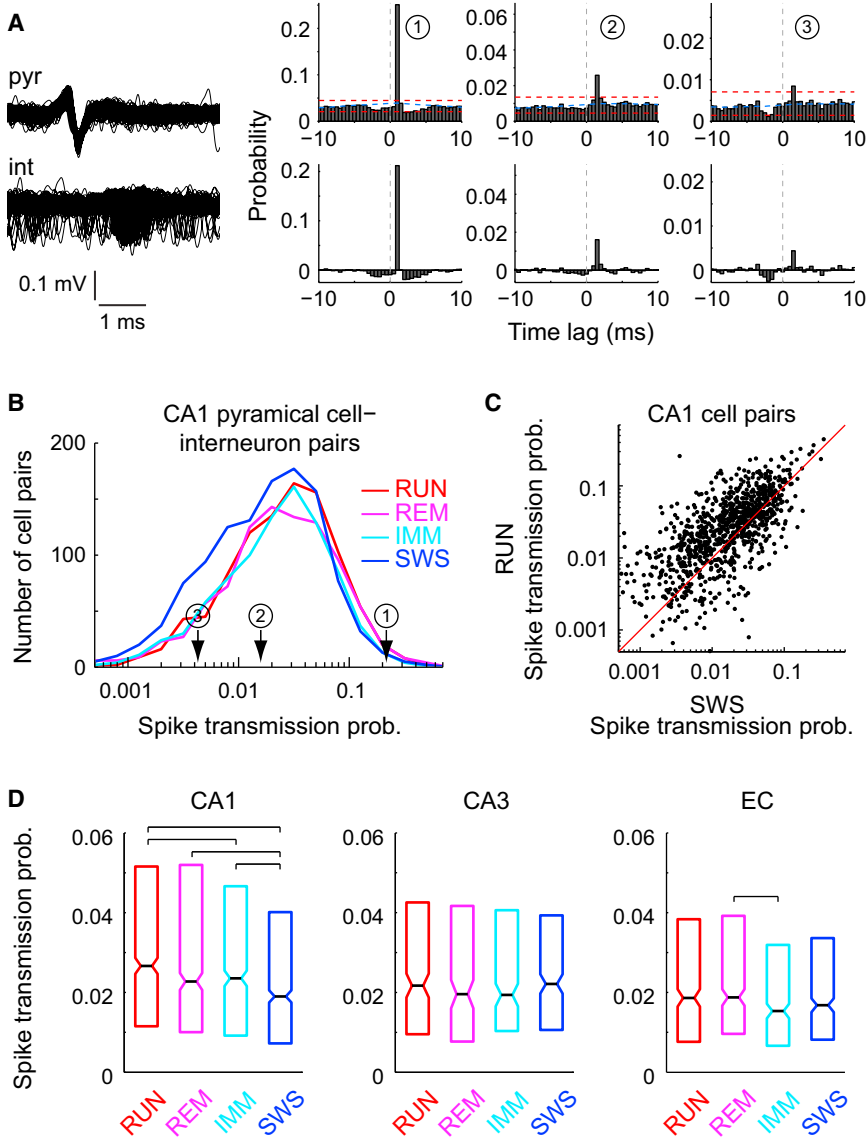


**Figure 7. Spike Transmission Probability Distributions in Different Brain States**

(A) Monosynaptic drive of a putative interneuron by a pyramidal cell. Left: superimposed filtered waveforms (800 Hz to 5 kHz) of a pyramidal cell (pyr) and an interneuron (int) triggered by spiking of a pyramidal cell. The two neurons were recorded from different silicon probe shanks. Right: three example cross-correlograms showing short-latency, putative monosynaptic interactions between CA1 pyramidal-interneuron pairs (recorded from two different electrodes). The first example corresponds to the left filtered waveforms. Dashed red lines indicate 0.1% and 99.9% global confidence intervals estimated by spike jittering at a uniform interval of [−5, 5] ms (Fujisawa et al., 2008); blue, mean. Note the different magnitude probability scales. Bottom row: shuffling corrected histograms of the same neuron pairs.

(B) Distribution of spike transmission probability values (note log scale) between CA1 pyramidal cells and putative interneurons in different brain states. Circled numbers indicate the probability values shown in (A).

(C) Comparison of spike transmission probability between RUN and SWS. Note larger values during RUN. Each dot represents a single cell pair.

(D) Spike transmission probability between principal cells and putative interneurons in the CA1, CA3 regions and EC (neuron pairs from EC layers were combined) in different brain states. Median, lower, and upper quartiles are shown. Brackets indicate significant differences ( $p < 0.05$ , Kruskal-Wallis ANOVA, followed by Tukey's honestly significant difference test).

See also Figure S7.

distribution of efficacy values (Figures 7B and S7A). Spike transmission efficacy was brain-state dependent, with the strongest efficacy during RUN and REM, and the weakest efficacy during SWS in CA1 (Figures 7C, 7D, and S7B;  $p < 0.05$ , Kruskal-Wallis ANOVA, followed by Tukey's honestly significant difference test).

Overall, these findings support the hypothesis that synaptic weight distribution is strongly skewed in the cortex (Song et al., 2005; Sayer et al., 1990; Mitra et al., 2012).

## DISCUSSION

We have found that the distribution of firing rates, burst discharges, and spike transmission probability between principal cells and interneurons have an approximately lognormal distribution in the EC and hippocampus. In all regions and layers examined, the firing-rate distribution was skewed in all brain states. Firing rates and bursts were correlated across brain states, between familiar environments, and even between familiar and novel environments. The magnitude of population synchrony during ripple events, reflecting the network-level cooperation of many individual neurons, was also strongly

the assumption that the magnitude of spike transmission, as measured in short-time spike cross-correlations, is proportional to the synaptic weight between them (Figure 7A; Experimental Procedures; Mizuseki et al., 2009; Fujisawa et al., 2008; Marshall et al., 2002; Barthó et al., 2004; Maurer et al., 2006; Dupret et al., 2013). Of the 32,406 principal neuron-interneuron cell pairs examined, 2,163 showed significant peaks within <4 ms (CA1 = 1,183 of 17,234; CA 3 = 368 of 6,412; EC = 612 of 8,760 cell pairs). The magnitude of the peak (i.e., the excess numbers of postsynaptic spikes divided by the number of pre-synaptic spikes, reflecting the efficacy of spike transmission probability) of the cross-correlogram was taken as a proxy for the synaptic strength between the neurons (Figure 7A).

Spike transmission efficacy showed a large variability across pairs, with the majority of pairs weakly coupled and a small minority strongly coupled, as quantified by the lognormal-like

skewed. These findings suggest that a preconfigured, skewed firing-rate distribution of the population is a robust and important aspect of cortical computation.

### A Preserved Minority of Neurons Is Active in All Brain States and Environments

Hippocampal neurons in different environments typically “remap,” and thus the firing-rate population vectors in each situation are unique (Leutgeb et al., 2005; Muller and Kubie, 1987; Samsonovich and McNaughton, 1997). Against this background, the highly conserved firing rates across brain states and testing situations are surprising but not exclusive. Our findings thus indicate that such environment-induced changes are superimposed on relatively stable discharge rates of individual neurons.

An unexpected finding of our experiments is that a minority of highly active and bursting neurons are responsible for nearly half of the spikes in any time window. This highly active subgroup may be responsible for a reliable propagation of activity in multiple layers of the feed-forward EC-hippocampal network (Mizuseki et al., 2009). Equally important is our observation that the remaining half of the action potentials in a given time window is contributed by a very large fraction of slow-discharging neurons. The activity of this majority may be critical for optimal performance. In addition, the slow-firing majority may serve to provide excitation to interneurons and thereby secure a sufficient level of inhibition to counter the effects of the fast-firing minority. Such a balance mechanism may be essential to maintain a self-organized, sustained activity in large-scale networks. In support of this hypothesis, a skewed distribution of synaptic weights has been shown to be critical for stabilizing neuronal circuits in tissue cultures (Mitra et al., 2012), and elimination of either a large fraction of weakly coupled and slow-firing neurons or a minority of very active cells was sufficient to abort ongoing network activity in computer models (Ikegaya et al., 2012; Izhikevich et al., 2004). In the present experiments, brain state and environmental influences affected mostly slow-firing neurons, in line with previous observations (Dragoi et al., 2003). Sleep may be a critical state to differentially affect slow-firing neurons and weak synaptic connections while preserving the strongly firing minority “core” (Tononi and Cirelli, 2006; Grosmark et al., 2012). It remains for future research to identify the conditions that may convert slowly discharging neurons to highly active ones and vice versa (Hirase et al., 2001; Battaglia et al., 2005; Mankin et al., 2012; Ziv et al., 2013).

### Skewed Distribution of Spike Transmission Probability

How does the lognormal pattern of firing rates arise? A suggested possibility is that many highly efficient synapses converge on a minority of cells (Barth and Poulet, 2012; Koulakov et al., 2009; Loewenstein et al., 2011). Indeed, the distribution of synaptic strengths between cortical cells is strongly skewed (Song et al., 2005; Ikegaya et al., 2012; Sayer et al., 1990; Feldmeyer et al., 2002; Arellano et al., 2007). Such a large variation of synaptic efficacy can be structurally related to the lognormal distribution of dendritic spine sizes of cortical neurons (Loewenstein et al., 2011). Our findings regarding the skewed distribution of spike transmission probability between pyramidal cells and interneurons provide further support for this idea. A second

possibility is a disproportional distribution of excitatory and inhibitory inputs to neurons (Yassin et al., 2010). An additional source of rate variability may be the skewed distribution of membrane conductances across neurons (Narayanan and Johnston, 2012). The lognormal-like distribution of burst rates supports the latter hypothesis since burst occurrence depends largely on the intrinsic properties of neurons (Harris et al., 2001; Jarsky et al., 2008). In light of previous observations (Yassin et al., 2010), our findings suggest that the rate distribution of principal neurons may also indicate how neurons are embedded in cortical circuits. Targeted recordings from fosGFP transgenic mice *in vivo* showed that neurons that had previously expressed c-fos, and thus were labeled by GFP, fired faster than nonlabeled neurons in layer 2/3 of primary sensory cortex. Importantly, the highly active fosGFP<sup>+</sup> neurons were connected to each other more frequently than fosGFP<sup>-</sup> neurons (Yassin et al., 2010), suggesting that the high-firing and strongly bursting minority may form special highly active subnetworks.

### CONCLUSIONS

The skewed distribution of the discharge rate of cortical neurons has important consequences for the interpretation of neuronal interactions. First, lumped models of cortical operations using neurons with “representative” activity cannot adequately describe network functions because there is no physiologically meaningful “mean” or “typical” rate for cortical neurons. Second, hypotheses about sparse and energy-efficient coding mechanisms should be supported by recordings from large populations of neurons because the mean rates of a small group of cells cannot describe the true population behavior of neurons or predict the mechanisms that bring about the activation of their targets (Mizuseki et al., 2009). Third, comparisons of mean rate distributions across testing conditions should not use statistics that require Gaussian distribution as a precondition. Fourth, high-firing-rate neurons are important because they carry more information. Reducing the spike rates of fast-firing neurons led to a loss of their advantage in spatial coherence, stability, and spatial information rate, indicating that the source of their gain is their high-frequency firing. The highly active minority and the slow-firing majority may be wired differently or possess highly distinct intrinsic biophysical properties (Barth and Poulet, 2012; Dragoi and Tonegawa, 2011; Lee et al., 2012). An important goal for future research is to explore the physiological mechanisms that underlie the continuum of the lognormal rule of synaptic efficacy and firing-rate distributions, and to elucidate how gene expression and molecular, morphological, and circuit properties interact with the firing rate of each neuron.

### EXPERIMENTAL PROCEDURES

#### Animals and Surgery

Eleven male Long-Evans rats (250–400 g) were implanted with a four- or eight-shank silicon probe in the right dorsal hippocampus under isoflurane anesthesia (1%–1.5%) and recorded from dorsal CA1 pyramidal layers. In four of the rats, another four-shank silicon probe was also implanted in the right dorsocaudal medial EC (Mizuseki et al., 2009). The silicon probes were attached to micromanipulators and moved slowly to the target. Each shank had eight recording sites (160  $\mu\text{m}^2$  each site, 1–3  $M\Omega$  impedance) and the

intershank distance was 200  $\mu\text{m}$ . The recording sites were staggered to provide a two-dimensional arrangement (20  $\mu\text{m}$  vertical separation). The EC probe was positioned so that the different shanks were recorded from different layers (Mizuseki et al., 2009). At the end of the physiological recordings, a small anodal DC current (2–5  $\mu\text{A}$ , 10 s) was applied to the recording sites 1 or 2 days before the animals were sacrificed. The rats were deeply anesthetized and perfused with 10% formalin solution. The position of the electrodes was confirmed histologically as previously described (Mizuseki et al., 2009; Diba and Buzsáki, 2008). Two stainless-steel screws inserted above the cerebellum were used as indifferent and ground electrodes during recordings. All protocols were approved by the institutional animal care and use committees of Rutgers University and New York University.

#### Behavioral Testing

After the animals recovered from surgery (~1 week), physiological signals were recorded during six different types of active waking behaviors: (1) On an elevated linear track (250 cm  $\times$  7 cm), the animals were required to run back and forth to obtain a 30  $\mu\text{l}$  water reward at both ends (Mizuseki et al., 2009). (2) In the open field task, the rats chased randomly dispersed drops of water or pieces of Froot Loops (~25 mg; Kellogg's) on an elevated square platform (180 cm  $\times$  180 cm, or 120 cm  $\times$  120 cm; Mizuseki et al., 2009). (3) The rewarded wheel-running task and (4) the alternation task in the T-maze (100 cm  $\times$  120 cm) with wheel running delay were described previously (Mizuseki et al., 2009; Pastalkova et al., 2008). The tasks on (5) an elevated plus maze (100 cm  $\times$  100 cm) and (6) a zigzag maze (100 cm  $\times$  200 cm) with 11 corridors were described previously (Mizuseki et al., 2009, 2012). Theta periods from all maze behaviors were lumped together as "RUN". Recordings were also carried out during sleep, typically both before and after tasks, in the animal's home cage. The maze was regarded as "novel" when the animal performed the task on it for the first time and "familiar" after at least three testing sessions.

#### Data Collection and Cell-Type Classification

Detailed information about the recording system and spike sorting is available elsewhere (Mizuseki et al., 2009; Diba and Buzsáki, 2008; Csicsvari et al., 1999). Briefly, signals were amplified (1,000 $\times$ ), band-pass filtered (1 Hz to 5 kHz), and acquired continuously at 20 kHz (DataMax system; RC Electronics) or 32 kHz (NeuraLynx, MT) at 16-bit resolution. After recording, the signals were downsampled to 1,250 Hz for the LFP analysis. Positive polarity is up in all illustrations. To maximize the detection of very slowly discharging ("silent") neurons (Thompson and Best, 1989), clustering was performed on concatenated files of several behavioral and sleep sessions recorded at the same electrode position on the same day. Spike sorting was performed automatically using KlustaKwik (<http://klustakwik.sourceforge.net>), followed by manual adjustment of the clusters (Klusters software package, <http://klusters.sourceforge.net>). After spike sorting, the spike features of units as a function of time were plotted, and the units and sessions with signs of significant drift over the period of recording were discarded. For the remaining data, only units with clear refractory periods and well-defined cluster boundaries were included in the analyses (Harris et al., 2000, 2001).

Classification of principal neurons and interneurons of hippocampal and EC neurons was described previously (Mizuseki et al., 2009). A total of 3,541 (CA1), 962 (CA3), 66 (DG), 491 (EC2), 576 (EC3), and 559 (EC5) principal neurons, and 468 (CA1), 216 (CA3), 52 (DG), 85 (EC2), 217 (EC3), and 94 (EC5) interneurons were identified and used for analyses. The tip of the probe either moved spontaneously or was moved by the experimenter between recording days. However, we cannot exclude the possibility that some neurons recorded on different days were identical because spikes recorded on each day were clustered separately.

#### Detection of Brain States

Theta periods during task performance (RUN), IMM, REM epochs (REM), and SWS were detected using the ratio of the power in the theta band (6–10 Hz) to the delta band (1–4 Hz) of LFP, followed by manual adjustment with the aid of visual inspection of whitened power spectra and the raw traces (Mizuseki et al., 2011, 2012). The manual adjustment was necessary to remove falsely detected short segments of data and epochs containing movement artifacts.

REM periods were cross-validated with notes taken by the experimenter while observing theta activity online in a sleep session and verifying that the rat was sleeping. The total recording times were  $57.4 \pm 36.1$  min for RUN,  $20.8 \pm 13.2$  min for REM,  $40.0 \pm 23.2$  min for IMM, and  $114.7 \pm 59.5$  min for SWS (mean  $\pm$  SD).

#### Spiking Activity during Sharp Wave Ripples

To detect ripple events, LFP in CA1 pyramidal layer during nontheta periods was band-pass filtered (140–230Hz), and the power (root-mean-square) was calculated in 17 ms sliding time windows. A ripple epoch was defined as a period during which the ripple power was continuously greater than the mean + 3 SD, and the peak of power in the period was greater than the mean + 7 SD. Results were similar when we used five different thresholds (mean + 7, 6, 5, 4, or 3 SD for peak of power, and mean + 3, 2.5, 2, 1.8, or 1.5 SD for the start and end of the epochs, respectively). Events shorter than 15 ms were discarded. The mean rates of detected ripple events (number of events per minute, mean  $\pm$  SD) were  $16.1 \pm 3.4$ ,  $20.3 \pm 4.1$ ,  $25.5 \pm 4.8$ ,  $32.5 \pm 5.6$ , and  $43.8 \pm 6.9$  during SWS, and  $4.7 \pm 3.5$ ,  $6.6 \pm 4.2$ ,  $9.5 \pm 4.9$ ,  $14.6 \pm 6.2$ , and  $24.5 \pm 10.9$  during IMM (mean + 7, 6, 5, 4, or 3 SD for peak power threshold).

To quantify the spiking activity of individual CA1 neurons during SPW-Rs, we used the following three measurements for SWS and IMM separately: (1) the proportion of spikes during SPW-Rs, defined as the number of spikes during SPW-Rs divided by the number of all the spikes; (2) the proportion of SPW-Rs in which a neuron fired, defined as the number of SPW-Rs in which the neuron fired at least once, divided by the total number of SPW-Rs; and (3) the mean number of spikes per SPW-R, which was obtained by dividing the number of spikes during SPW-Rs by the total number of SPW-Rs.

To quantify the magnitude of the CA1 pyramidal neurons' synchrony during SPW-Rs, only sessions with >50 simultaneously recorded CA1 pyramidal neurons were used. To calculate the proportion of CA1 pyramidal cells that fired at least once during a ripple, the number of neurons that fired during a ripple epoch was divided by the number of simultaneously recorded neurons during the session.

To quantify the magnitude of the CA1 (or CA3) pyramidal neurons' synchrony in each brain state, only sessions with >40 simultaneously recorded CA1 (or CA3) pyramidal neurons were used. To calculate the proportion of CA1 (or CA3) pyramidal cells that fired at least once in 10, 20, 50, 100, or 200 ms bins, the number of neurons that fired in each time bin was divided by the number of simultaneously recorded neurons during the session.

#### Bursts and Firing Rate

A burst event was defined as a series of three or more spikes with <8 ms interspike intervals. A burst index was defined as the ratio of spikes in bursts to all spikes. To calculate the burst-event rate, the number of burst events was divided by the recording time for each brain state. To fit the firing rate to the lognormal distribution, the maximum-likelihood method was used.

#### Spatial Tuning of Spiking Activity

Data recorded on the open field (180 cm  $\times$  180 cm or 120 cm  $\times$  120 cm) and linear track (250 cm) were used to analyze the spatial tuning of spiking activity. Only the data obtained during theta epochs were used. The position of the animal was estimated by recording LEDs on the head stage at 30 Hz. For the linear track, the positions were projected onto the track axis. The position and spiking data were sorted into 5 cm  $\times$  5 cm (open field) or 5 cm (linear track) bins, generating the raw maps of spike number and occupancy. A raw rate map was constructed by dividing a raw spike map by a raw occupancy map, and used to compute spatial coherence. Gaussian kernel (SD = 5 cm) was applied for both raw maps of spike and occupancy, and then a smoothed rate map was constructed by dividing the smoothed spike map by the smoothed occupancy map. The peak and mean firing rates in the place field, number of place fields, stability, and spatial information rate were computed from the smoothed rate map.

A place field was defined as a contiguous region of at least 225  $\text{cm}^2$  (nine bins) for the open field and 15 cm (three bins) for the linear track where the firing rate was >10% of the peak rate in the maze and the peak firing rate of the area was >2 Hz, and the special coherence of the region was >0.7. Using a

threshold of 20% of the peak rate and omitting the special coherence criteria gave similar results (Figure S3).

Spatial coherence (Muller and Kubie, 1989) was defined as the correlation between a list of firing rates in each pixel and a corresponding list of firing rates averaged over the adjacent pixels of each pixel, and measures the local smoothness of the firing rate in space (Muller and Kubie, 1989; Hafting et al., 2008; Mizuseki et al., 2009) (eight adjacent pixels for the open fields, two adjacent pixels for the linear track). Spatial coherence of each candidate place field was calculated using the firing rate map of the region and used to define a place field. Spatial coherence of each neuron was calculated using the entire firing rate map in the maze and used in Figure 4B. Place map stability was defined by the pixel-by-pixel correlation coefficient between the firing-rate maps of the first and second halves of the recording session.

For the linear track, spatial representation (rate map, spatial coherence, and phase precession) was analyzed for each direction separately. The area at 0–25 cm (the starting point) was excluded from the analysis to exclude the effect of behavioral variability. To quantify the degree of phase precession, place fields were identified on the linear track using >2 Hz peak firing rate, >10% peak firing rate, and >0.7 spatial coherence as criteria (Hafting et al., 2008; Mizuseki et al., 2009). Place fields with fewer than 50 spikes and fields that included the turning position of the track were discarded (Hafting et al., 2008; Mizuseki et al., 2009). The theta phases of spikes were displayed as a function of the distance from the start of the place field, and the theta phase-position correlation was determined by parametrically rotating the phase by the position matrix for each place field. Phase rows were shifted by 1° steps from 0° to 360°. For each rotation, a linear regression curve was fitted. The slope of the regression line at the phase rotation that gave the largest explained variance R<sup>2</sup> was used as the degree of phase precession (degree per centimeter). In some cases, this objective and automatic method gives a spurious positive slope value even when visual inspection suggests a negative slope (Hafting et al., 2008; Mizuseki et al., 2009).

The spatial information rate (bits per second) (Skaggs et al., 1993) was calculated according to the following formula:

$$\text{Information rate} = \sum_{i=1}^N p_i \lambda_i \log_2 \frac{\lambda_i}{\bar{\lambda}}$$

where  $i = 1, \dots, N$  represents pixel identification number,  $p_i$  is the probability of occupancy of pixel  $i$ ,  $\lambda_i$  is the mean firing rate of pixel  $i$ , and  $\bar{\lambda}$  is the overall mean firing rate of the cell on the maze.

#### Probability of Spike Transmission

First, the principal cell-interneuron pairs with putative monosynaptic excitation were identified by cross-correlogram analysis (Fujisawa et al., 2008) using all spikes recorded during all brain states. Although the validity of this method should be strengthened by rigorous experiments, the available evidence, obtained by intracellular recordings and optogenetic activation of principal cells, supports its use (Marshall et al., 2002; Quilichini et al., 2010; Stark et al., 2012). Cross-correlation histograms were normalized by dividing the spike count in each bin by the number of reference spikes, yielding the probability of the referred neurons' spikes given the reference event. Monosynaptic excitation between cell pairs was detected by a nonparametric significance test based on jittering of spike trains as described previously in detail (Fujisawa et al., 2008). Briefly, for each cell pair, each spike from each neuron in the original data set was randomly and independently jittered at a uniform interval of [−5, +5] ms to form a surrogate data set. The process was repeated independently 1,000 times to form 1,000 such surrogate data sets. Then, the cross-correlograms were constructed for surrogate data sets as a function of latency across an interval of [−20, +20] ms (Fujisawa et al., 2008). Global bands at an acceptance level of 99.9% were constructed for the cross-correlogram from the maximum and minimum of each jitter surrogate cross-correlogram across the interval [−20, +20] ms. The short-latency peak bin(s) in the original cross-correlogram was determined to be statistically significant (at  $p < 0.001$ ) when the probabilities in the bin(s) in the cross-correlogram were atypical with respect to the global bands anywhere at the latency [1, 4] ms. For cell pairs recorded from the same electrode, the 0–1 ms bin was not considered,

because our clustering program cannot resolve superimposed spikes. After using the jittering method, we visually inspected all cell pairs that were identified as monosynaptically connected pairs and excluded spurious cell pairs (e.g., an erroneously identified pair caused by potential contamination of spikes between units of the pair recorded from the same silicon probe shank) from further analysis.

To estimate the spike transmission probability for each brain state, we used only cell pairs in which both neurons fired more than 20 times and the number of events in the interval [−20, +20] ms in the original cross-correlogram was larger than 100 in that brain state. For each cell pair with significant monosynaptic excitation, the same jitter method described above was applied 1,000 times and the mean cross-correlogram of surrogate data sets was calculated for each brain state. The excess of probabilities in the original cross-correlogram over the mean of the surrogate cross-correlogram in the short-latency significant peak bin(s) was taken as the probability of monosynaptic transmission.

Data analysis was carried out using custom-written MATLAB-based software.

#### SUPPLEMENTAL INFORMATION

Supplemental Information includes seven figures and can be found with this article online at <http://dx.doi.org/10.1016/j.celrep.2013.07.039>.

#### ACKNOWLEDGMENTS

We thank K. Diba and E. Pastalkova for sharing their data, and Kenneth Harris, Christof Koch, Jeff Magee, Alex Reyes, Eric Schomburg, and Richard Tsien for comments. This work was supported by the National Institutes of Health (NS034994, MH54671, and NS074015), the National Science Foundation (SBE 0542013), the J.D. McDonnell Foundation, the Uehara Memorial Foundation (K.M.), the Astellas Foundation for Research on Metabolic Disorders (K.M.), and the Japan Society of Promotion for Sciences (K.M.).

Received: February 21, 2013

Revised: July 15, 2013

Accepted: July 26, 2013

Published: August 29, 2013

#### REFERENCES

- Arellano, J.I., Benavides-Piccione, R., Defelipe, J., and Yuste, R. (2007). Ultrastructure of dendritic spines: correlation between synaptic and spine morphologies. *Front. Neurosci.* 1, 131–143.
- Barth, A.L., and Poulet, J.F. (2012). Experimental evidence for sparse firing in the neocortex. *Trends Neurosci.* 35, 345–355.
- Barthó, P., Hirase, H., Monconduit, L., Zugaro, M., Harris, K.D., and Buzsáki, G. (2004). Characterization of neocortical principal cells and interneurons by network interactions and extracellular features. *J. Neurophysiol.* 92, 600–608.
- Battaglia, F.P., Sutherland, G.R., Cowen, S.L., McNaughton, B.L., and Harris, K.D. (2005). Firing rate modulation: a simple statistical view of memory trace reactivation. *Neural Netw.* 18, 1280–1291.
- Buzsáki, G., Horváth, Z., Urioste, R., Hetke, J., and Wise, K. (1992). High-frequency network oscillation in the hippocampus. *Science* 256, 1025–1027.
- Csicsvari, J., Hirase, H., Czurkó, A., Mamiya, A., and Buzsáki, G. (1999). Oscillatory coupling of hippocampal pyramidal cells and interneurons in the behaving Rat. *J. Neurosci.* 19, 274–287.
- Csicsvari, J., Hirase, H., Mamiya, A., and Buzsáki, G. (2000). Ensemble patterns of hippocampal CA3-CA1 neurons during sharp wave-associated population events. *Neuron* 28, 585–594.
- Diba, K., and Buzsáki, G. (2008). Hippocampal network dynamics constrain the time lag between pyramidal cells across modified environments. *J. Neurosci.* 28, 13448–13456.
- Dragoi, G., and Tonegawa, S. (2011). Preplay of future place cell sequences by hippocampal cellular assemblies. *Nature* 469, 397–401.

- Dragoi, G., Harris, K.D., and Buzsáki, G. (2003). Place representation within hippocampal networks is modified by long-term potentiation. *Neuron* 39, 843–853.
- Dupret, D., O'Neill, J., and Csicsvari, J. (2013). Dynamic reconfiguration of hippocampal interneuron circuits during spatial learning. *Neuron* 78, 166–180.
- Feldmeyer, D., Lübke, J., Silver, R.A., and Sakmann, B. (2002). Synaptic connections between layer 4 spiny neurone-layer 2/3 pyramidal cell pairs in juvenile rat barrel cortex: physiology and anatomy of interlaminar signalling within a cortical column. *J. Physiol.* 538, 803–822.
- Fujisawa, S., Amarasingham, A., Harrison, M.T., and Buzsáki, G. (2008). Behavior-dependent short-term assembly dynamics in the medial prefrontal cortex. *Nat. Neurosci.* 11, 823–833.
- Grosmark, A.D., Mizuseki, K., Pastalkova, E., Diba, K., and Buzsáki, G. (2012). REM sleep reorganizes hippocampal excitability. *Neuron* 75, 1001–1007.
- Hafting, T., Fyhn, M., Molden, S., Moser, M.B., and Moser, E.I. (2005). Microstructure of a spatial map in the entorhinal cortex. *Nature* 436, 801–806.
- Hafting, T., Fyhn, M., Bonnevie, T., Moser, M.B., and Moser, E.I. (2008). Hippocampus-independent phase precession in entorhinal grid cells. *Nature* 453, 1248–1252.
- Harris, K.D., Henze, D.A., Csicsvari, J., Hirase, H., and Buzsáki, G. (2000). Accuracy of tetrode spike separation as determined by simultaneous intracellular and extracellular measurements. *J. Neurophysiol.* 84, 401–414.
- Harris, K.D., Hirase, H., Leinekugel, X., Henze, D.A., and Buzsáki, G. (2001). Temporal interaction between single spikes and complex spike bursts in hippocampal pyramidal cells. *Neuron* 32, 141–149.
- Hirase, H., Leinekugel, X., Czurkó, A., Csicsvari, J., and Buzsáki, G. (2001). Firing rates of hippocampal neurons are preserved during subsequent sleep episodes and modified by novel awake experience. *Proc. Natl. Acad. Sci. USA* 98, 9386–9390.
- Hromádka, T., Deweese, M.R., and Zador, A.M. (2008). Sparse representation of sounds in the unanesthetized auditory cortex. *PLoS Biol.* 6, e16.
- Ikegaya, Y., Sasaki, T., Ishikawa, D., Honma, N., Tao, K., Takahashi, N., Minamisawa, G., Ujita, S., and Matsuki, N. (2012). Interpyramidal spike transmission stabilizes the sparseness of recurrent network activity. *Cereb. Cortex*.
- Izhikevich, E.M., Gally, J.A., and Edelman, G.M. (2004). Spike-timing dynamics of neuronal groups. *Cereb. Cortex* 14, 933–944.
- Jarsky, T., Mady, R., Kennedy, B., and Spruston, N. (2008). Distribution of bursting neurons in the CA1 region and the subiculum of the rat hippocampus. *J. Comp. Neurol.* 506, 535–547.
- Koulakov, A.A., Hromádka, T., and Zador, A.M. (2009). Correlated connectivity and the distribution of firing rates in the neocortex. *J. Neurosci.* 29, 3685–3694.
- Krupic, J., Burgess, N., and O'Keefe, J. (2012). Neural representations of location composed of spatially periodic bands. *Science* 337, 853–857.
- Lee, D., Lin, B.J., and Lee, A.K. (2012). Hippocampal place fields emerge upon single-cell manipulation of excitability during behavior. *Science* 337, 849–853.
- Leutgeb, S., Leutgeb, J.K., Barnes, C.A., Moser, E.I., McNaughton, B.L., and Moser, M.B. (2005). Independent codes for spatial and episodic memory in hippocampal neuronal ensembles. *Science* 309, 619–623.
- Levy, W.B., and Baxter, R.A. (1996). Energy efficient neural codes. *Neural Comput.* 8, 531–543.
- Lisman, J.E. (1997). Bursts as a unit of neural information: making unreliable synapses reliable. *Trends Neurosci.* 20, 38–43.
- Loewenstein, Y., Kuras, A., and Rumpel, S. (2011). Multiplicative dynamics underlie the emergence of the log-normal distribution of spine sizes in the neocortex *in vivo*. *J. Neurosci.* 31, 9481–9488.
- Magee, J.C., and Johnston, D. (1997). A synaptically controlled, associative signal for Hebbian plasticity in hippocampal neurons. *Science* 275, 209–213.
- Mankin, E.A., Sparks, F.T., Slayley, B., Sutherland, R.J., Leutgeb, S., and Leutgeb, J.K. (2012). Neuronal code for extended time in the hippocampus. *Proc. Natl. Acad. Sci. USA* 109, 19462–19467.
- Marshall, L., Henze, D.A., Hirase, H., Leinekugel, X., Dragoi, G., and Buzsáki, G. (2002). Hippocampal pyramidal cell-interneuron spike transmission is frequency dependent and responsible for place modulation of interneuron discharge. *J. Neurosci.* 22, RC197.
- Maurer, A.P., Cowen, S.L., Burke, S.N., Barnes, C.A., and McNaughton, B.L. (2006). Phase precession in hippocampal interneurons showing strong functional coupling to individual pyramidal cells. *J. Neurosci.* 26, 13485–13492.
- Mitra, A., Mitra, S.S., and Tsien, R.W. (2012). Heterogeneous reallocation of presynaptic efficacy in recurrent excitatory circuits adapting to inactivity. *Nat. Neurosci.* 15, 250–257.
- Mizuseki, K., Sirota, A., Pastalkova, E., and Buzsáki, G. (2009). Theta oscillations provide temporal windows for local circuit computation in the entorhinal-hippocampal loop. *Neuron* 64, 267–280.
- Mizuseki, K., Diba, K., Pastalkova, E., and Buzsáki, G. (2011). Hippocampal CA1 pyramidal cells form functionally distinct sublayers. *Nat. Neurosci.* 14, 1174–1181.
- Mizuseki, K., Royer, S., Diba, K., and Buzsáki, G. (2012). Activity dynamics and behavioral correlates of CA3 and CA1 hippocampal pyramidal neurons. *Hippocampus* 22, 1659–1680.
- Muller, R.U., and Kubie, J.L. (1987). The effects of changes in the environment on the spatial firing of hippocampal complex-spike cells. *J. Neurosci.* 7, 1951–1968.
- Muller, R.U., and Kubie, J.L. (1989). The firing of hippocampal place cells predicts the future position of freely moving rats. *J. Neurosci.* 9, 4101–4110.
- Narayanan, R., and Johnston, D. (2012). Functional maps within a single neuron. *J. Neurophysiol.* 108, 2343–2351.
- O'Connor, D.H., Peron, S.P., Huber, D., and Svoboda, K. (2010). Neural activity in barrel cortex underlying vibrissa-based object localization in mice. *Neuron* 67, 1048–1061.
- Olshausen, B.A., and Field, D.J. (1997). Sparse coding with an overcomplete basis set: a strategy employed by V1? *Vision Res.* 37, 3311–3325.
- O'Keefe, J., and Nadel, L. (1978). *The Hippocampus as a Cognitive Map* (Oxford: Oxford University Press).
- O'Keefe, J., and Recce, M.L. (1993). Phase relationship between hippocampal place units and the EEG theta rhythm. *Hippocampus* 3, 317–330.
- Pastalkova, E., Itskov, V., Amarasingham, A., and Buzsáki, G. (2008). Internally generated cell assembly sequences in the rat hippocampus. *Science* 321, 1322–1327.
- Pike, F.G., Meredith, R.M., Olding, A.W., and Paulsen, O. (1999). Rapid report: postsynaptic bursting is essential for 'Hebbian' induction of associative long-term potentiation at excitatory synapses in rat hippocampus. *J. Physiol.* 518, 571–576.
- Quilichini, P., Sirota, A., and Buzsáki, G. (2010). Intrinsic circuit organization and theta-gamma oscillation dynamics in the entorhinal cortex of the rat. *J. Neurosci.* 30, 11128–11142.
- Roxin, A., Brunel, N., Hansel, D., Mongillo, G., and van Vreeswijk, C. (2011). On the distribution of firing rates in networks of cortical neurons. *J. Neurosci.* 31, 16217–16226.
- Samsonovich, A., and McNaughton, B.L. (1997). Path integration and cognitive mapping in a continuous attractor neural network model. *J. Neurosci.* 17, 5900–5920.
- Sayer, R.J., Friedlander, M.J., and Redman, S.J. (1990). The time course and amplitude of EPSPs evoked at synapses between pairs of CA3/CA1 neurons in the hippocampal slice. *J. Neurosci.* 10, 826–836.
- Shadlen, M.N., and Newsome, W.T. (1998). The variable discharge of cortical neurons: implications for connectivity, computation, and information coding. *J. Neurosci.* 18, 3870–3896.
- Skaggs, W.E., McNaughton, B.L., Gothard, K.M., and Markus, E.J. (1993). An information-theoretic approach to deciphering the hippocampal code. In *Advances in Neural Information Processing Systems, Volume 5*, S.J. Hanson, J.D. Cowan, and C.L. Giles, eds. (Burlington, MA: Morgan Kaufmann), pp. 1030–1037.
- Song, S., Sjöström, P.J., Reigl, M., Nelson, S., and Chklovskii, D.B. (2005). Highly nonrandom features of synaptic connectivity in local cortical circuits. *PLoS Biol.* 3, e68.

- Stark, E., Koos, T., and Buzsáki, G. (2012). Diode probes for spatiotemporal optical control of multiple neurons in freely moving animals. *J. Neurophysiol.* **108**, 349–363.
- Thomas, M.J., Watabe, A.M., Moody, T.D., Makhinson, M., and O'Dell, T.J. (1998). Postsynaptic complex spike bursting enables the induction of LTP by theta frequency synaptic stimulation. *J. Neurosci.* **18**, 7118–7126.
- Thompson, L.T., and Best, P.J. (1989). Place cells and silent cells in the hippocampus of freely-behaving rats. *J. Neurosci.* **9**, 2382–2390.
- Thomson, A.M. (2000). Facilitation, augmentation and potentiation at central synapses. *Trends Neurosci.* **23**, 305–312.
- Tononi, G., and Cirelli, C. (2006). Sleep function and synaptic homeostasis. *Sleep Med. Rev.* **10**, 49–62.
- Wolfe, J., Houweling, A.R., and Brecht, M. (2010). Sparse and powerful cortical spikes. *Curr. Opin. Neurobiol.* **20**, 306–312.
- Yassin, L., Benedetti, B.L., Jouhanneau, J.S., Wen, J.A., Poulet, J.F., and Barth, A.L. (2010). An embedded subnetwork of highly active neurons in the neocortex. *Neuron* **68**, 1043–1050.
- Ziv, Y., Burns, L.D., Cocker, E.D., Hamel, E.O., Ghosh, K.K., Kitch, L.J., El Gamal, A., and Schnitzer, M.J. (2013). Long-term dynamics of CA1 hippocampal place codes. *Nat. Neurosci.* **16**, 264–266.